Environmental Science & Technology

Article

pubs.acs.org/est

Estimation of Size-Resolved Ambient Particle Density Based on the Measurement of Aerosol Number, Mass, and Chemical Size Distributions in the Winter in Beijing

Min Hu,*[,†] Jianfei Peng,[†] Kang Sun,[†] Dingli Yue,[†] Song Guo,[†] Alfred Wiedensohler,[‡] and Zhijun Wu[†,‡]

[†]State Key Joint Laboratory of Environmental Simulation and Pollution Control, College of Environmental Sciences and Engineering, Peking University, Beijing, People's Republic of China

[‡]Leibniz−Institute for Tropospheric Research, Leipzig, Germany

Supporting Information

ABSTRACT: Simultaneous measurements of aerosol size, distribution of number, mass, and chemical compositions were conducted in the winter of 2007 in Beijing using a Twin Differential Mobility Particle Sizer and a Micro Orifice Uniform Deposit Impactor. Both material density and effective density of ambient particles were estimated to be 1.61 ± 0.13 g cm^{-3} and 1.62 ± 0.38 g cm^{-3} for $PM_{1.8}$ and 1.73 ± 0.14 g cm^{-3} and 1.67 ± 0.37 g cm^{-3} for PM_{10}. Effective density decreased in the nighttime, indicating the primary particles emission from coal burning influenced the density of ambient particles. Size-resolved material density and effective density showed that both values increased with diameter from about 1.5 g cm^{-3} at the size of 0.1 μm to above 2.0 g cm^{-3} in the coarse mode. Material density was significantly higher for particles between 0.56 and 1.8 μm during clean episodes. Dynamic Shape Factors varied within the range of 0.95−1.13 and decreased with particle size, indicating that coagulation and atmospheric aging processes may change the shape of particles.

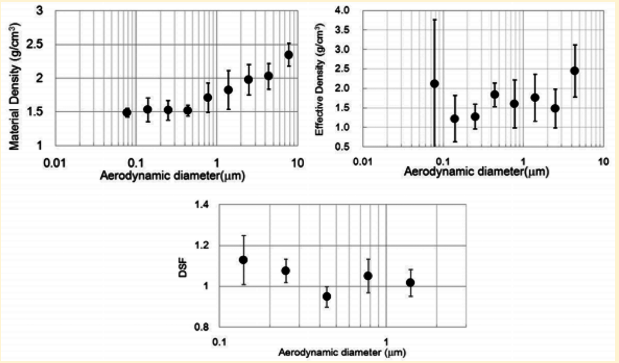

INTRODUCTION

Atmospheric particles are important components in ambient air because of their significant effects on air quality, human health, regional visibility, and global climate change.[1−3] These effects strongly depend on their size distribution, chemical compositions, and morphology. The properties of atmospheric particles may vary with their sources and change through aging processes in the atmosphere. For these complex properties of aerosols, the particle density can act as a good predictor.[4] Density is required to determine the relationship between mobility and aerodynamic diameter and to convert high time-resolved ambient particle number distribution to mass concentration related with air quality and visibility.[5,6] Furthermore, variations in particle density can be used to infer the mechanism of aerosol formation; effective density can reflect morphology information of particles. A size-resolved density of fine particles can also serve as a crude tracer for chemical composition and atmospheric processing and may play an important role when considering the associations between ambient particles and health effects.[4]

Several approaches to estimate particle density have been developed in the past. Generally, particle chemical compositions were used to derive the material density.[5,7] The application of high resolution online and in situ measurement techniques has been developed to estimate particle density. For example, a size distribution system such as a tandem differential mobility analyzer (TDMA), aerodynamic particle sizer (APS), differential mobility particle spectrometer (DMPS), or laser aerosol spectrometer (LAS-X)[8] can provide diameter information, and tapered element oscillating microbalance (TEOM) system,[4,6] aerosol particle mass (APM) analyzer system,[9,10] or aerosol time-of-flight mass spectrometer (ATOFMS)[11] can yield the mass information of particles. The combination of some of these systems has been reported in the literatures for calculating the effective particle density. The particle effective density can be deduced by combining mobility and aerodynamic diameter measurements.[12,13] However, the majority of the previous studies focused on laboratory generated particles. Recently, several studies to characterize the average density of fine particles or density of a selected diameter in the atmosphere have been reported in the literature;[4,8,14] yet only a few studies on the size-resolved density in the ambient air have been published so far,[14] especially size-resolved density in the mega-cities of developing countries.

Received: November 14, 2011
Revised: March 20, 2012
Accepted: March 29, 2012
Published: March 29, 2012

Atmospheric particulate pollution in the megacity of Beijing is a major concern, regarding the regional and urban air quality[15] as well as human health. Due to the industrial pattern and urbanization of Beijing, there are complex sources of primary aerosols which contain abundant chemical compositions with great varying range. Previous studies have provided a rough estimate of ambient particle density at values of 1.50 g/cm^3 for $PM_{2.5}$[16] and 1.68 g/cm^3 for PM_{10}.[17] However, these works did not consider the particle density in different size ranges. In the present study, we measured particle number size distributions and size-resolved mass/chemical compositions at Peking University (PKU), an urban site in Beijing, during the winter of 2007, employing a TDMPS-APS setup and Micro-Orifice Uniform Deposit Impactor (MOUDI). The day-to-day variability of both material density and effective density were assessed in terms of meteorological conditions and level of pollution. Additionally, the size-resolutions of both densities were estimated. Finally, the differences of size-resolved material and effective densities in different episodes were explored, and particle dynamic shape factors (DSF) were calculated.

METHODOLOGY

Methods To Estimate Particle Densities. Several density estimation methods have been developed on the basis of particle properties (mass, mobility, and/or aerodynamic diameter) and the flow regime (transition, free-molecular regime),[18] in which material and effective densities are two major approximations of true particle density.[19]

Material density (ρ_m) is the average density of the solid and liquid material in the particle. Assuming that volumes of species coexisting in an individual particle do not change upon mixing, the density of an internally mixed particle can be calculated using the material densities and mass concentrations of particulate constituents;[5,19]

$$\rho_m = \frac{\sum_{species} m_i}{\sum_{species} V_i} = \frac{\sum_{species} m_i}{\sum_{species} \frac{m_i}{\rho_i}} = \frac{\sum_{species} MC_i}{\sum_{species} \frac{MC_i}{\rho_i}} \quad (1)$$

where ρ_i is the material density of species i, V_i is its volume, m_i is its mass, and MC_i is its mass concentration. This approach is based on the assumption that there is no void space enclosed within the particle envelope. Hence, material density is larger than true particle density with internal voids in particles.

Effective density (ρ_{eff}) is defined as the ratio of the measured particle mass (m_p) to the particle volume calculated assuming a spherical particle with a diameter equal to the measured mobility diameter (d_m):[19]

$$\rho_{eff} = \frac{m_p}{\frac{\pi}{6} d_m^{\ 3}} \quad (2)$$

Substituting particle mass (MC) and volume concentration (VC) for mass and volume of a single particle in the eq 2, average apparent density within a certain size range can be obtained as follows:

$$\rho_{eff} = \frac{MC_{d_1}^{d_2}}{VC_{d_1}^{d_2}} = \frac{MC_{d_1}^{d_2}}{\frac{\pi}{6}\int_{d_1}^{d_2} d_p^3 \times n(d_p)\, d\, d_p} \quad (3)$$

where $n(d_p)$ is number concentration within a certain size range (d_1, d_2).

Effective density reflects both particle density and shape information. If the particles are spheres in absence of internal void, then the effective density equals the material density. If particles are not spherical, then the calculated volume or volume concentration surpasses the true values and the effective density is less than true particle density and definitely less than the material density.

The Dynamic Shape Factor (DSF), χ is defined as the ratio of the drag force on a spherical particle to the drag force on a spherical particle with a volume equivalent diameter d_{ve}.[11] It reflects irregularity of particles. The DSF is equal to 1 for spheres, and below 1.26 for compact structure of spheres.[11]

Effective density for irregular shaped particles can be overestimated by a factor approximately equal to the cube of DSF.[20] Assuming that material density equals to particle density, we can get an approximate value of DSF using material and effective density:

$$\chi = \frac{d_m}{d_{ve}} \frac{C_c(d_{ve})}{C_c(d_m)} = \left(\frac{\rho_p}{\rho_{eff}}\right)^{1/3} \frac{C_c(d_{ve})}{C_c(d_m)} \quad (3)$$

where C_c represents the Cunningham slip correction factor for a certain diameter.

Measurement Site and Instrumentation. The measurement was conducted in the winter in Beijing from January 22 to 27, 2007. The sampling site was on the rooftop of a six-floor building at the campus of Peking University (39°59′21″N, 116°18′25″ E), located in the northwestern urban area of Beijing.[21] The inlet of sampling system was placed 20 m above ground level. The surrounding objects were mainly teaching or office buildings. A major street lay on the east of the site, in a distance of about 250 m. No significant stationary emission sources were located nearby.

Two micro orifice uniform deposit impactors (MOUDI−110) (MSP Corporation, U.S.) were used to collect size-segregated aerosols with totally 10 size range from 0.056 to 18 μm (aerodynamic diameter) for the analysis of mass and chemical components.[22,23] The 50% cut points for each size range were 10, 5.6, 3.2, 1.8, 1.0, 0.56, 0.32, 0.18, 0.1, and 0.056 μm, respectively. The sampling time was separated into daytime (local Beijing time 8:00−19:00) and nighttime (local Beijing time 20:00−7:00 of the next day). In total, 11 sets of samples were obtained, with each set of samples including Ten Teflon filters and Ten Quartz filters. Before and after sampling, Teflon filters were weighed in Peking University's clean room after 24 h conditioning under constant temperature (20 ± 1 °C) and RH (40 ± 3%). Filters were put in the Petri dishes and stored in the refrigerator at the temperature of −20 °C.

Teflon samples were extracted by 10 mL pure water through an ultrasonic bath at temperature below 30 °C for 30 min, and analyzed by ion-chromatograph. The analysis methods were the same as some previous studies[22] and can be obtained in the Supporting Information. Ions we used in this study included NH_4^+, Na^+, K^+, Mg^{2+}, Ca^{2+}, F^-, Cl^-, NO_3^-, and SO_4^{2-}. Quartz filters were used for EC and OC concentrations analyzed using a thermal/optical transmittance aerosol carbon analyzer (Sunset ECOC).[24] The heating process of Sunset ECOC can be found in the Supporting Information. A laser transmittance signal was used to separate the carbon evolving in these final combustion steps into EC and OC. Field blank and lab blank were considered and all sampling concentrations were revised by blank concentration.

dx.doi.org/10.1021/es204073t | Environ. Sci. Technol. 2012, 46, 9941−9947

In this study, the species of the particles were sorted into SNA (sum of sulfate, nitrate and ammonium), other ions (sum of Na^+, K^+, Ca^{2+}, Mg^{2+}, Cl^-, F^-), EC (elemental carbon), OM (organic matter), and minerals. Concentrations of Organic matters (OM) were achieved through multiplying OC concentration by 1.4, and minerals were defined as mass concentrations subtracted by ions, EC and OM. The densities of chemical species for SNA, other ions, EC and OM, used in the calculation of the material density were 1.75, 2.0, 2.0, and 1.2 g cm^{-3}, respectively, according to previous studies.[5,25−27] Density of minerals was calculated as 2.8 g cm^{-3} based on the concentrations of elements (such as Si, Fe, Al, and Ca) in Beijing, and the densities of their molecular forms.[27,28]

Aerosol number size distributions between 3 nm and 10 μm were measured by a Twin Differential Mobility Particle Sizer (TDMPS) combined with aerodynamic particle sizer (APS) system. TDMPS was used to measure particles number concentration with mobility diameter under 700 nm. Meanwhile, APS could obtain a particle number concentration with an aerodynamic diameter above 600 nm. The relative humidity within the systems was kept below 30% by adding a silica-gel dryer in the inlet line and also in the sheath air cycle to reduce the RH dependence of the measured properties. Before measurement, flow rates of DMA, CPC, and APS were carefully measured and corrected if necessary. Size-dependent diffusional and gravitational losses for the inlet line were corrected using the empirical functions for laminar flow.[29] Diffusional loss inside the equipment and multicharged effect were corrected by the software of instrument. Further descriptions of the TDMPS-APS system were previously presented.[17,30]

In this study, we employed TDMPS data to describe size distribution of aerosols under 690 nm (mobility diameter) and APS data to describe size distribution above 690 nm (mobility diameter). To calculate the volume concentrations above 690 nm (mobility diameter), aerodynamic diameters from APS system were converted to mobility diameters using the following equation:

$$d_m = d_{ve}\rho_{eff}^{1/2} \approx d_{ve}\rho_m^{1/2} \quad (4)$$

The material density was used as the particle density to convert aerodynamic diameter of APS to mobility diameter. For example, material density calculated from chemical composition in the size of 1.0−1.8 μm of MOUDI was used to convert aerodynamic diameter within 1.0 to 1.8 μm to mobility diameter. The same equation was applied when converting mobility diameter of TDMPS to aerodynamic diameter.

RESULTS AND DISCUSSION

Classification and Properties of Particulate Pollution Episodes. During the measurement period from January 22 to 27, 2007, the temperature generally remained below 10 °C and the relative humidity below 40%, so the hygroscopic growth of aerosols could be neglected. No precipitation occurred during this period. NOAA "HYSPIT 4.9" backward trajectory model[31] was introduced to classify the different episodes. The 24 h backward trajectories terminated on a height of 200 m above the ground at 0:00 and 12:00 local time. Each trajectory represented one sampling period, either daytime or nighttime. Backward trajectories were grouped by assigning to two clusters using a k-means cluster algorithm. On the basis of PM_{10} pollution level and the backward trajectory cluster analysis, the measurement period was divided into one polluted episode (January 22 daytime to 25 daytime) and one clean episode (January 25 nighttime to 27 daytime) (Figure 1), in which

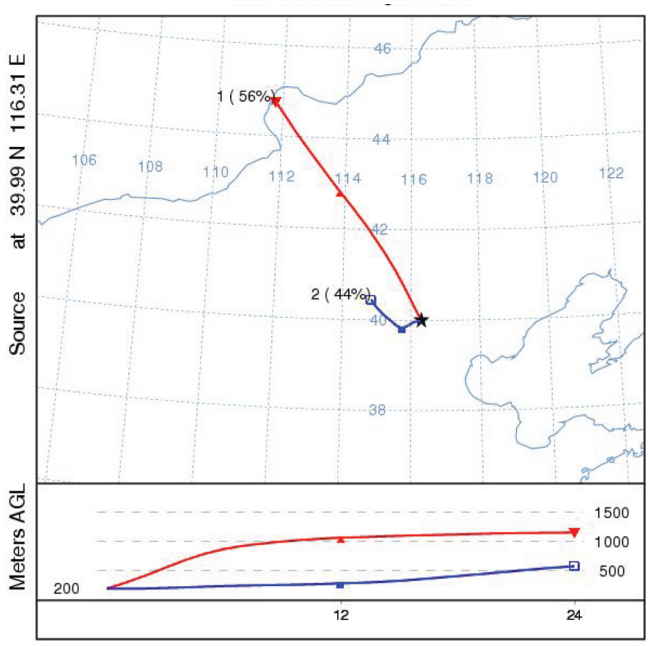

Figure 1. Mean 24-h backward trajectories of polluted (blue line) and clean (red line) episodes based on HYSPIT clustering model.

average PM_{10} concentrations were 192 μg m^{-3} and 54 μg m^{-3}, respectively. The backward trajectories of the polluted episode originated from the surrounding area of Beijing, indicating that stagnant air mass was transported slowly. The origins of backward trajectories in clean episode were mostly in arid area far north of Beijing.

Size-resolved mass and chemical compositions obtained by the MOUDI analysis exhibited distinct features during the polluted and clean episodes (Figure 2). The mass size distributions showed a bimodal feature with peaks in the size range of 0.56−1 μm and 3.2−5.6 μm and the cutoff size between fine and coarse particles in the size range of 1.8−3.2 μm. Therefore, the diameter of 1.8 μm was defined as the cut point that split fine and coarse particles in this study.[23]

Generally speaking, fine particles were dominant in PM_{10}, accounting for 70% of mass concentration in average during wintertime in Beijing. OM and EC represented considerable proportions in fine particle mass, accounting for 43.9 ± 14.5% and 7.4 ± 2.0%, respectively, whereas secondary inorganic ions (SNA) corresponded to 24.2 ± 5.3% of $PM_{1.8}$. Seasonal variation of particulate OC in Beijing showed that the highest OC concentration occurred in winter mainly owing to extra coal burning for the heating supply, low temperature avoiding OC evaporation and inversion enhancing pollution accumulation.[32] Equivalent concentrations of SO_4^{2-} and NO_3^- correlated very well with that of NH_4^+ (with R^2 = 0.97 and slope = 1.01), suggesting that SNA were mostly in the form of $(NH_4)_2SO_4$ and NH_4NO_3. The peaks of mass concentration as well as concentrations of chemical components (such as SNA, EC, and OM) were in the size range of 0.32−0.56 μm in both polluted and clean episodes. Mineral dust was the main component in coarse particles, according for 40−75% of coarse particles, especially higher during the clean episode.

dx.doi.org/10.1021/es204073t | Environ. Sci. Technol. 2012, 46, 9941−9947

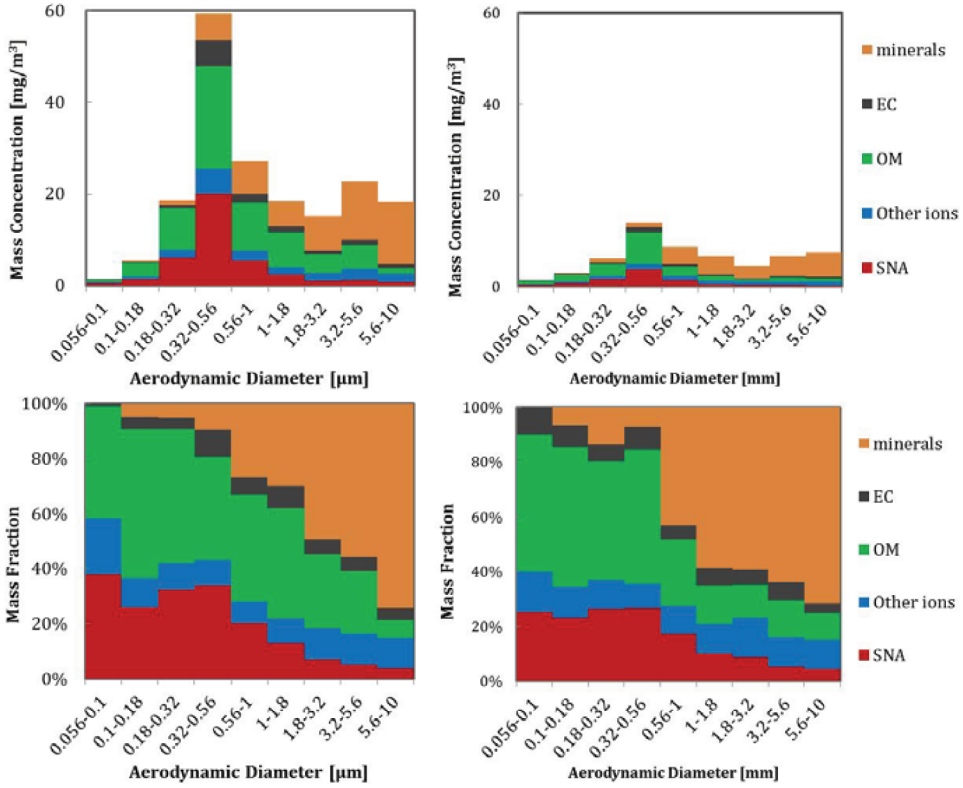

Figure 2. Size distribution of mass and chemical compositions in polluted (left) and clean (right) episodes.

Table 1. Summary of the Aerosol Mass, Volume and Density during the Measurement

	size range	mass conc (μg m^{-3})	volume conc (cm^3 m^{-3})	material density (g cm^{-3})	effective density (g cm^{-3})
average	$PM_{1.8}$	97.5	69.3	1.61 ± 0.13[a]	1.62 ± 0.38
	$PM_{1.8-10}$	28.2	15.6	2.09 ± 0.15	1.93 ± 0.56
	PM_{10}	125.7	84.9	1.73 ± 0.14	1.67 ± 0.37
polluted episode	$PM_{1.8}$	130.5	96.4	1.55 ± 0.05	1.42 ± 0.16
	$PM_{1.8-10}$	37.8	21.3	2.03 ± 0.09	1.80 ± 0.40
	PM_{10}	168.3	117.7	1.66 ± 0.06	1.48 ± 0.15
clean episode	$PM_{1.8}$	39.8	21.8	1.63 ± 0.08	1.96 ± 0.42
	$PM_{1.8-10}$	11.3	5.7	2.18 ± 0.21	2.15 ± 0.80
	PM_{10}	51.0	27.5	1.78 ± 0.14	2.01 ± 0.41

[a]Average concentration ± standard deviation.

Material Density and Effective Density of Fine and Coarse Particles. The material density of particles was calculated with the particle chemical composition. During the winter measurement period, the mean material density for $PM_{1.8}$, $PM_{1.8-10}$, and PM_{10} were 1.61 ± 0.13 g cm^{-3}, 2.09 ± 0.15, and 1.73 ± 0.14 g cm^{-3}, respectively (Table 1). Material density in the coarse mode was found significant higher than in fine particles as there were more resuspended road dust and other fugitive dust with relatively higher density in the coarse mode. Effective density of $PM_{1.8}$ and PM_{10} was estimated based on the methods described in eq 3. The mean effective densities for $PM_{1.8}$, $PM_{1.8-10}$, and PM_{10} were 1.62 ± 0.38 g cm^{-3}, 1.93 ± 0.56 g cm^{-3}, and 1.67 ± 0.37 g cm^{-3}, respectively. The concentrations were comparable with the material densities, justifying the use material density in the conversion between aerodynamic diameter and mobility diameter of APS.

Both material and effective densities of $PM_{1.8}$ in the whole sampling period together with $PM_{1.8}$ mass concentrations are provided in Figure 3. Uncertainty analysis of both densities was conducted in mass weighting, ions and EC/OC analyzing, TDMPS/APS measurement, as well as the density assumption of each chemical group. The methods to calculate uncertainty can be found in the Supporting Information. The material density of fine particles showed no obvious trend during the measurement, with the value varying from 1.54 to 1.76 g cm^{-3}. The effective density, however, displayed an opposite tendency with the mass concentration, which meant lower polluted episodes and higher clean episodes. The higher percentage of mineral components might be the reason for this phenomenon. Besides, the effective density of $PM_{1.8}$ always decreased in the nighttime while the material density showed no diurnal variation. In Beijing, trucks are only allowed to enter the fifth ring road at midnight and coal combustion for domestic heating is more important in the nighttime than in the daytime. Large amounts of chain agglomerate particles emitting from coal burning and diesel emission might decrease the density of ambient particles.

dx.doi.org/10.1021/es204073t | Environ. Sci. Technol. 2012, 46, 9941−9947

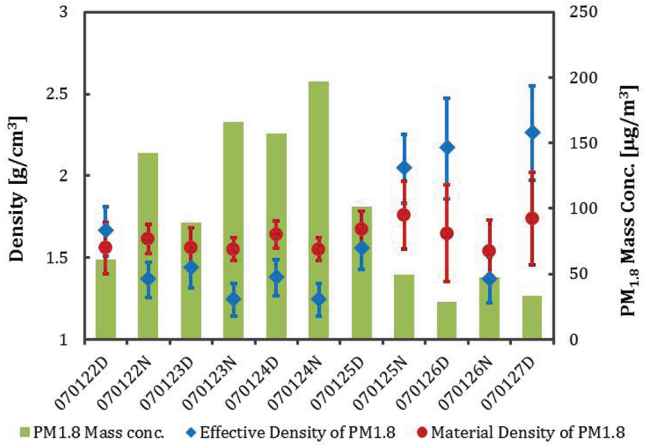

Figure 3. Time series of material and effective density of fine particles together with $PM_{1.8}$ mass concentration. Error bars are the evaluated uncertainties of density. Time format of X coordinate is yymmdd, with D and N referring to daytime and nighttime, respectively.

Material density is not influenced by the mixing condition and shape of particles and has a relative smaller fluctuation. Nevertheless, to measure and estimate chemical compositions of particles is time-consuming, and sampling artifacts in filter methods are difficult to avoid. On the contrary, long-term and high time resolution effective density data are obtained more easily. As a result, the studies on particle densities in recent years mainly focused on the effective density. The density values evaluated in this work agreed well with those reported in other studies. For example, Khlystov et al. reported that effective density and material density were about 1.5 g cm^{-3} for $PM_{2.5}$ in the urban atmosphere of Pittsburgh.[33] Hand and Kreidenweis estimated the effective density of 1.56 ± 0.12 g cm^{-3} for the region of southwest Texas.[27] In the urban site in Augsburg, average densities in summer and winter were 1.68 g cm^{-3} and 1.60 g cm^{-3}, respectively.[4] In Riverside, a receptor site of Los Angeles, the Geller's measured that effective densities were 1.2−1.5 g cm^{-3} for 50−202 nm particles.[14]

Size-Resolved Material and Effective Densities. Size-resolved material densities derived for the MOUDI are shown in Figure 4(a). Material densities were flattened at a value of 1.5 g cm^{-3} over the particle diameter from 0.056 to 0.56 μm, as organic matters and SNA were the dominant species in theses size ranges and their percentages in mass did not change much in these stages. In the size ranges of 0.56−1 μm and 1−1.8 μm, the material density was higher in the clean episode. In the clean episode, a strong wind would resuspend dust from the ground, making mineral dust dominant in larger stages of fine particles, resulting in a remarkable increase of material densities from the size range of 0.56−1 μm. However, in polluted episode, organic matters and SNA were abundant in fine particles and were more likely to grow into larger size, resulting in lower material densities in the size ranges of 0.56−1 μm and 1−1.8 μm. Because of the abundance of minerals in coarse particles in Beijing,[23,28] material densities of coarse modes in both clean and polluted episodes exceeded 2.0 g cm^{-3}.

On the basis of size-resolved material density, the effective density within the same size range can be calculated using the method described in eq 3. Results of the effective density are shown in Figure 4(b). As APS might have a lower efficiency for large particles above 6 μm,[34] the effective density in the size range of 5.6−10 μm can be overestimated and is not shown in the figure. Generally, the effective density showed a similar value to the material density within the corresponding size range. Nevertheless, the differences were still obvious. The density of the final stage (0.056−0.1 μm) had a rather large standard deviation, implying a significant estimation error. Because the sampling loadings of the final stage of MOUDI (0.056−0.1 μm) were rather low (about 30 μg on average), random errors of mass concentration (about 29 μg) derived from the differences in the weights of the filters before and after sampling could be up to 100%. The particle bounce from the larger sizes was also a possible explanation for this random error.[33] Furthermore, most ions in this stage were under the detection limit (detection limit of each ion can be found in ref 23). These resulted in the large standard deviation of the size range of 0.056−0.1 μm. With respect to the other size ranges

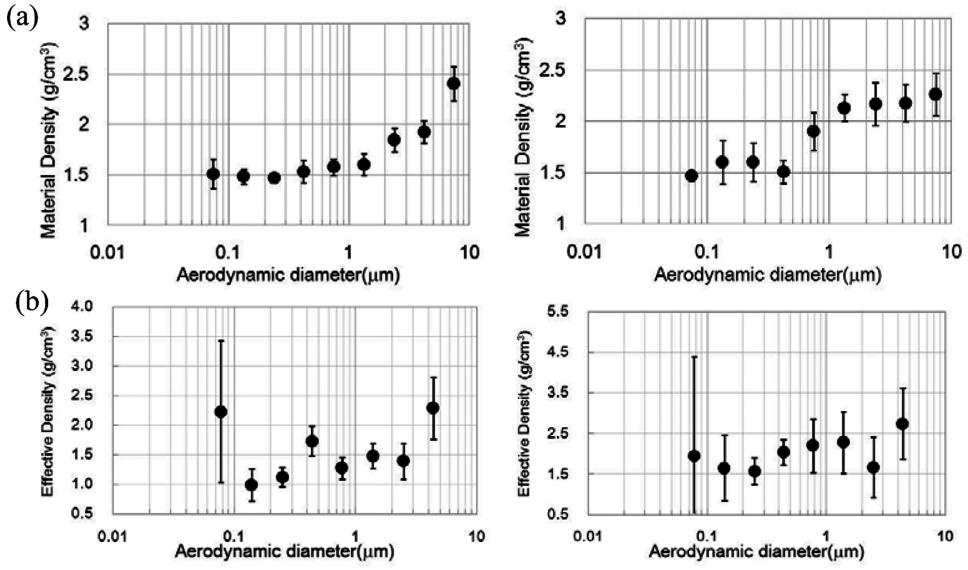

Figure 4. Size-resolved material density (a) and effective density (b) in polluted episodes (left) and clean episodes (right). Error bars of each stage represent the standard deviation in different sampling episodes.

dx.doi.org/10.1021/es204073t | Environ. Sci. Technol. 2012, 46, 9941−9947

under 1.8 μm, effective densities were substantially lower than corresponding material density in fine particles. However, if the particle contained internal voids, then the material density was larger than the true particle density because gaseous components with zero density were not taken into account. In addition, according to the definition, the effective density was dependent on both particle density and shape effect. For nonspherical particles, the effective density was less than particle density, i.e., $\rho_{eff} \leq \rho_m \leq \rho_p$ with the equality being valid only to spherical particles in the absence of internal voids.

Effective density is not only dependent on the composition of particles, but is also related closely to the morphology of particles. Irregularly shaped particles with large DSF may have substantially low effective density, in spite of much higher material density. Previous work focusing on measuring the effective density of diesel or soot particles concluded that when particles become more irregular and agglomerated, they show much lower effective density.[35] Since there was a large fluctuation of calculated DSF in this size range (0.056−0.1 μm), the DSFs of particles from 0.1 to 1.8 μm were estimated using eq 4 based on the size-resolved effective and material density. The results are displayed in Figure 5.

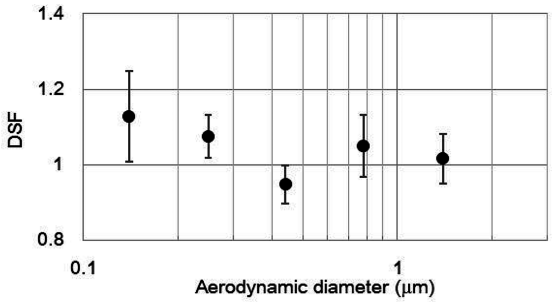

Figure 5. Dynamic Shape Factors of fine particles in the winter of 2007.

DSFs were estimated to vary within the range of 0.95−1.13 in the urban atmosphere. The Spearman's rank correlation was introduced to study the relationship between DSF and particle diameter. The Spearman correlation coefficient is a nonparametric measure of statistical dependence between two variables, providing an assessement on the relationship between two variables to be described by a nonlinear monotonic function. Assuming that there was no correlation between DSF and particle diameter for 55 total sets of data, the Spearman correlation coefficient ρ is −0.281, indicating that DSF significantly decreased over the diameter at the 5% significance level. The present work is the first measurement of DSF in a megacity, indicating the morphology change of particles.

In the winter in Beijing, coal combustion for the heating supply contributes most importantly to particulate matter.[36] Large quantities of primary black carbon and organic carbon are emitted into atmosphere. Previous laboratory study has shown that the DSF of fresh soot could be as high as 3.0 at about 100 nm. Coating of organic compounds on soot aerosols could significantly increase effective density and as a result decrease the DSF.[10] As particles grow larger, their shape may change due to coagulation and atmospheric aging, which contribute to scavenge gas phase components and make particles more compact.[4] Consequently, aged particles may show smaller DSF, approaching the value of 1.0. In addition, particle alignment in the electric field of DMA also affects their DSF. In order to select particles with a larger mobility diameter, a higher DMA voltage is needed. These particles tend to orient parallel in stronger electric field, and reveal lower DSF than smaller particles of the same shape, which tend to orient randomly.[11]

■ ASSOCIATED CONTENT

Supporting Information

Detailed information including introduction of the ion-chromatograph, heating process of Sunset ECOC, overlap of TDMPS/APS, and methods to calculate the uncertainty. This material is available free of charge via the Internet at http://pubs.acs.org.

■ AUTHOR INFORMATION

Corresponding Author

*Phone: 86-10-62759880; fax: 86-10-62751920; e-mail: minhu@pku.edu.cn.

Notes

The authors declare no competing financial interest.

■ ACKNOWLEDGMENTS

This work is supported by the National Natural Science Foundation of China (20977001, 21025728), and also supported by the China Ministry of Environmental Protection's Special Funds for Scientific Research on Public Welfare (201009002). The author would like to thank Renyi Zhang and Alexei F. Khalizov from Texas A&M University for their contribution to this work.

■ REFERENCES

(1) Laden, F.; Neas, L. M.; Dockery, D. W.; Schwartz, J. Association of fine particulate matter from different sources with daily mortality in six US cities. *Environ. Health Perspect.* **2000**, *108* (10), 941−947.

(2) Dockery, D. W.; Pope, C. A. Acute respiratory effects of particulate air-pollution. *Annu. Rev. Publ. Health* **1994**, *15*, 107−132.

(3) *IPCC, Intergovernmental Panel on Climate Change: Climate Change 2007: The Physical Science Basis*; Cambridge University Press: Cambridge, UK; 2007.

(4) Pitz, M.; Schmid, O.; Heinrich, J.; Birmili, W.; Maguhn, J.; Zimmermann, R.; Wichmann, H. E.; Peters, A.; Cyrys, J. Seasonal and diurnal variation of PM2.5 apparent particle density in urban air in Augsburg, Germany. *Environ. Sci. Technol.* **2008**, *42* (14), 5087−5093.

(5) McMurry, P. H.; Wang, X.; Park, K.; Ehara, K. The relationship between mass and mobility for atmospheric particles: A new technique for measuring particle density. *Aerosol Sci. Technol.* **2002**, *36* (2), 227−238.

(6) Morawska, L.; Johnson, G.; Ristovski, Z. D.; Agranovski, V. Relation between particle mass and number for submicrometer airborne particles. *Atmos. Environ.* **1999**, *33* (13), 1983−1990.

(7) Hasan, H.; Dzubay, T. G. Apportioning light extinction coefficients to chemical-species in atmospheric aerosol. *Atmos. Environ.* **1983**, *17* (8), 1573−1581.

(8) Pitz, M.; Cyrys, J.; Karg, E.; Wiedensohler, A.; Wichmann, H. E.; Heinrich, J. Variability of apparent particle density of an urban aerosol. *Environ. Sci. Technol.* **2003**, *37* (19), 4336−4342.

(9) Zhang, R. Y.; Khalizov, A. F.; Pagels, J.; Zhang, D.; Xue, H. X.; McMurry, P. H. Variability in morphology, hygroscopicity, and optical properties of soot aerosols during atmospheric processing. *Proc. Natl. Acad. Sci. U.S.A.* **2008**, *105* (30), 10291−10296.

(10) Xue, H. X.; Khalizov, A. F.; Wang, L.; Zheng, J.; Zhang, R. Y. Effects of coating of dicarboxylic acids on the mass-mobility relationship of soot particles. *Environ. Sci. Technol.* **2009**, *43* (8), 2787−2792.

(11) Zelenyuk, A.; Cai, Y.; Imre, D. From agglomerates of spheres to irregularly shaped particles: Determination of dynamic shape factors

from measurements of mobility and vacuum aerodynamic diameters. *Aerosol Sci. Technol.* **2006**, *40* (3), 197−217.
(12) Malloy, Q. G. J.; Nakao, S.; Qi, L.; Austin, R.; Stothers, C.; Hagino, H.; Cocker, D. R. Real-time aerosol density determination utilizing a modified scanning mobility particle sizer-aerosol particle mass analyzer system. *Aerosol Sci. Technol.* **2009**, *43* (7), 673−678.
(13) Spencer, M. T.; Shields, L. G.; Prather, K. A. Simultaneous measurement of the effective density and chemical composition of ambient aerosol particles. *Environ. Sci. Technol.* **2007**, *41* (4), 1303−1309.
(14) Geller, M.; Biswas, S.; Sioutas, C. Determination of particle effective density in urban environments with a differential mobility analyzer and aerosol particle mass analyzer. *Aerosol Sci. Technol.* **2006**, *40* (9), 709−723.
(15) Jung, J.; Lee, H.; Kim, Y. J.; Liu, X. G.; Zhang, Y. H.; Hu, M.; Sugimoto, N., Optical properties of atmospheric aerosols obtained by in situ and remote measurements during 2006 Campaign of Air Quality Research in Beijing (CAREBeijing-2006). *J. Geophys. Res.−Atmos.* **2009**, *114*.
(16) Gao, J.; Zhou, Y.; Wang, T.; Wang, W. Inter-comparison of WPS-TEOM-MOUDI and investigation on particle density. *Environ. Sci. (in Chinese)* **2007**, *28* (9), 1929−1934.
(17) Yue, D. L.; Hu, M.; Wu, Z. J.; Wang, Z. B.; Guo, S.; Wehner, B.; Nowak, A.; Achtert, P.; Wiedensohler, A.; Jung, J.; Kim, Y. J.; Liu, S. Characteristics of aerosol size distributions and new particle formation in the summer in Beijing. *J. Geophys. Res.−Atmos.* **2009**, *114*, -.
(18) Schmid, O.; Karg, E.; Hagen, D. E.; Whitefield, P. D.; Ferron, G. A. On the effective density of non-spherical particles as derived from combined measurements of aerodynamic and mobility equivalent size. *J. Aerosol Sci.* **2007**, *38* (4), 431−443.
(19) DeCarlo, P. F.; Slowik, J. G.; Worsnop, D. R.; Davidovits, P.; Jimenez, J. L. Particle morphology and density characterization by combined mobility and aerodynamic diameter measurements. Part 1: Theory. *Aerosol Sci. Technol.* **2004**, *38* (12), 1185−1205.
(20) Zelenyuk, A.; Yang, J.; Song, C.; Zaveri, R. A.; Imre, D. A new real-time method for determining particles' sphericity and density: Application to secondary organic aerosol formed by ozonolysis of α-pinene. *Environ. Sci. Technol.* **2008**, *42* (21), 8033−8038.
(21) Wu, Z. J.; Hu, M.; Lin, P.; Liu, S.; Wehner, B.; Wiedensohler, A. Particle number size distribution in the urban atmosphere of Beijing, China. *Atmos. Environ.* **2008**, *42* (34), 7967−7980.
(22) Liu, S.; Hu, M.; Slanina, S.; He, L. Y.; Niu, Y. W.; Bruegemann, E.; Gnauk, T.; Herrmann, H. Size distribution and source analysis of ionic compositions of aerosols in polluted periods at Xinken in Pearl River Delta (PRD) of China. *Atmos. Environ.* **2008**, *42* (25), 6284−6295.
(23) Guo, S.; Hu, M.; Wang, Z. B.; Slanina, J.; Zhao, Y. L. Size-resolved aerosol water-soluble ionic compositions in the summer of Beijing: Implication of regional secondary formation. *Atmos. Chem. Phys.* **2010**, *10* (3), 947−959.
(24) Hu, M.; Deng, Z.; Wang, Y.; Lin, P.; Zeng, L.; Kondo, Y.; Yongjing, Z. Comparison of EC/OC in PM2.5 between filter sampling off-line analysis and in-situ online measurement. *Environ. Sci. (in Chinese)* **2008**, *29* (12), 3297−3303.
(25) Saarikoski, S.; Makela, T.; Hillamo, R.; Aalto, P. P.; Kerminen, V. M.; Kulmala, M. Physico-chemical characterization and mass closure of size-segregated atmospheric aerosols in Hyytiala, Finland. *Boreal Environ. Res.* **2005**, *10* (5), 385−400.
(26) Park, K.; Kittelson, D. B.; Zachariah, M. R.; McMurry, P. H. Measurement of inherent material density of nanoparticle agglomerates. *J. Nanopart. Res.* **2004**, *6* (2−3), 267−272.
(27) Hand, J. L.; Kreidenweis, S. M. A new method for retrieving particle refractive index and effective density from aerosol size distribution data. *Aerosol Sci. Technol.* **2002**, *36* (10), 1012−1026.
(28) Zhang, W. J.; Zhuang, G. S.; Guo, J. H.; Xu, D. Q.; Wang, W.; Baumgardner, D.; Wu, Z. Y.; Yang, W. Sources of aerosol as determined from elemental composition and size distributions in Beijing. *Atmos. Res.* **2010**, *95* (2−3), 197−209.
(29) Willeke, K.; Baron, P. A. *Aerosol Measurement Principles, Techniques, and Applications*; Van Nostrand Reinhold: Hoboken, NJ, 1993.
(30) Wu, Z. J.; Hu, M.; Liu, S.; Wehner, B.; Bauer, S.; Ssling, A. M.; Wiedensohler, A.; Petaja, T.; Dal Maso, M.; Kulmala, M. New particle formation in Beijing, China: Statistical analysis of a 1-year data set. *J. Geophys. Res.−Atmos.* **2007**, *112* (D9), -.
(31) Wu, Z. J.; Hu, M.; Shao, K. S.; Slanina, J. Acidic gases, NH(3) and secondary inorganic ions in PM(10) during summertime in Beijing, China and their relation to air mass history. *Chemosphere* **2009**, *76* (8), 1028−1035.
(32) Lin, P.; Hu, M.; Deng, Z.; Slanina, J.; Han, S.; Kondo, Y.; Takegawa, N.; Miyazaki, Y.; Zhao, Y.; Sugimoto, N. Seasonal and diurnal variations of organic carbon in PM2.5 in Beijing and the estimation of secondary organic carbon. *J. Geophys. Res.−Atmos.* **2009**, *114*, -.
(33) Khlystov, A.; Stanier, C.; Pandis, S. N. An algorithm for combining electrical mobility and aerodynamic size distributions data when measuring ambient aerosol. *Aerosol Sci. Technol.* **2004**, *38*, 229−238.
(34) Armendariz, A. J.; Leith, D. Concentration measurement and counting efficiency for the aerodynamic particle sizer 3320. *J. Aerosol Sci.* **2002**, *33* (1), 133−148.
(35) Park, K.; Cao, F.; Kittelson, D. B.; McMurry, P. H. Relationship between particle mass and mobility for diesel exhaust particles. *Environ. Sci. Technol.* **2003**, *37* (3), 577−583.
(36) Song, Y.; Tang, X.; Xie, S.; Zhang, Y.; Wei, Y.; Zhang, M.; Zeng, L.; Lu, S. Source apportionment of PM2.5 in Beijing in 2004. *J. Hazard. Mater.* **2007**, *146* (1−2), 124−130.